Research Paper

Disproportionate neuroanatomical effects of *DCC* haploinsufficiency in adolescence compared with adulthood: links to dopamine, connectivity, covariance, and gene expression brain maps in mice

Daniel Hoops, PhD; Yohan Yee, PhD; Christopher Hammill, MSc; Sammi Wong, BSc; Colleen Manitt, PhD; Barry J. Bedell, PhD; Lindsay Cahill, PhD; Jason P. Lerch, PhD; Cecilia Flores*, PhD; John G. Sled*, PhD

Background: Critical adolescent neural refinement is controlled by the DCC (deleted in colorectal cancer) protein, a receptor for the netrin-1 guidance cue. We sought to describe the effects of reduced *DCC* on neuroanatomy in the adolescent and adult mouse brain. **Methods:** We examined neuronal connectivity, structural covariance, and molecular processes in a *DCC*-haploinsufficient mouse model, compared with wild-type mice, using new, custom analytical tools designed to leverage publicly available databases from the Allen Institute. **Results:** We included 11 *DCC*-haploinsufficient mice and 16 wild-type littermates. Neuroanatomical effects of *DCC* haploinsufficiency were more severe in adolescence than adulthood and were largely restricted to the mesocorticolimbic dopamine system. The latter finding was consistent whether we identified the regions of the mesocorticolimbic dopamine system a priori or used connectivity data from the Allen Brain Atlas to determine de novo where these dopamine axons terminated. Covariance analyses found that *DCC* haploinsufficiency disrupted the coordinated development of the brain regions that make up the mesocorticolimbic dopamine system. Gene expression maps pointed to molecular processes involving the expression of *DCC*, *UNC5C* (encoding DCC's co-receptor), and *NTN1* (encoding its ligand, netrin-1) as underlying our structural findings. **Limitations:** Our study involved a single sex (males) at only 2 ages. **Conclusion:** The neuroanatomical phenotype of *DCC* haploinsufficiency described in mice parallels that observed in *DCC*-haploinsufficient humans. It is critical to understand the *DCC*-haploinsufficient mouse as a clinically relevant model system.

Background

Adolescence is a critical period for the maturation of complex cognitive functions like reward, motivation, and behavioural control.[1] This period is also characterized by the maturation of the nervous system, including the refinement of neuronal connectivity.[2] Some refinement is controlled by the DCC (deleted in colorectal cancer) protein, a receptor for the netrin-1 guidance cue (encoded by the *NTN1* gene).[3,4] In humans, *DCC* haploinsufficiency, resulting from 1 nonfunctional allele for the *DCC* gene, leads to altered behaviours.[5] Altered expression of *DCC* and *NTN1* is also implicated in psychiatric disorders, particularly those that emerge during adolescence.[6,7]

Mice that are haploinsufficient for the *DCC* gene have provided critical insight into the role of DCC receptors in adolescent brain development. These mice have reduced levels of DCC protein and altered neurodevelopmental processes, including altered mesolimbic dopamine axon innervation to the prefrontal cortex. By inducing conditional *DCC* haploinsufficiency in dopamine neurons in the ventral tegmental area, we showed that DCC receptors control the targeting of mesolimbic dopamine axons in adolescence, preventing them from growing ectopically to the prefrontal cortex.[8–10] Adult, but not adolescent, *DCC*-haploinsufficient mice have increased dopamine innervation and release in the prefrontal cortex, and, inversely, reduced dopamine varicosities and release in the

Correspondence to: C. Flores, 6875 Bd LaSalle, Verdun, Que., H4H 1R3; cecilia.flores@mcgill.ca. J.G. Sled, 170 Elizabeth Street, Toronto, Ont., M5G 1E8; john.sled@sickkids.ca.

*Equally credited senior authors.

Submitted July 31, 2023; Revised Jan. 23, 2024; Revised Feb. 23, 2024; Revised Mar. 6, 2924; Accepted Mar. 6, 2024

Cite as: *J Psychiatry Neurosci* 2024 May 1;49(3). doi: 10.1503/jpn.230106

nucleus accumbens.[9,11,12] Behaviours related to the function of the mesocorticolimbic dopamine system are altered in adulthood, including blunted responses to stimulant drugs of abuse.[8,12–15] Increased dopamine in the prefrontal cortex may underlie symptoms of several psychiatric disorders.[16]

Broadly, we sought to explore whether the neuroanatomical effects of *DCC* haploinsufficiency are general or specific to the mesocorticolimbic dopamine system and whether these effects are likely to be directly caused by changes in *DCC* expression or by downstream and compensatory changes in the expression of a wide constellation of genes. We conducted comparisons across the entire brain between *DCC*-haploinsufficient and wild-type mice in both adolescence and adulthood.

Methods

To compare the effects of *DCC* haploinsufficiency in and outside the mesocorticolimbic dopamine system, we used 2 approaches. First, we examined the regions we identified a priori as components of the mesocorticolimbic system and compared them with those that are not part of this system. We then used data sets from the Allen Brain Connectivity Atlas to compare the anatomic distribution of dopamine axons with the brain structure phenotype of *DCC* haploinsufficiency without any a priori information. We also examined whether the affected brain regions showed any developmental shifts in structural covariance caused by *DCC* haploinsufficiency, since their development is associated with the growth of dopamine axons to these regions.[3,6]

We then developed methods for integrating our data with that of the Allen Institute Spatial Gene Expression atlases, allowing us to examine potential molecular correlates of the neuroanatomical changes associated with *DCC* haploinsufficiency. We examined whether genes associated with netrin-1 signalling were more likely to be associated with the *DCC*-haploinsufficient phenotype than other genes, and whether genes expressed at different postnatal developmental time points showed varying relationships to the phenotype. These analyses could provide an idea of the mechanisms that link the *DCC*-haploinsufficient genotype with its neuroanatomical phenotype, both spatially and temporally.

Animals

Mice bearing 1 nonfunctional copy of the *DCC* gene on a C57BL/6J background (i.e., *DCC*-haploinsufficient mice)[17] were bred and maintained at the animal facility of the Douglas Hospital Research Centre in Montréal, Canada. They were maintained on a 12-hour light–dark cycle with ad libitum access to food and water. Pups were weaned at postnatal day 21 and housed in cages with same-sex littermates. The *DCC*-haploinsufficient and wild-type mice in this study were from the same litters and our experimental design counterbalanced for age and litter.

Image acquisition and processing

We conducted magnetic resonance imaging (MRI) of male *DCC*-haploinsufficient mice and wild-type littermates during adolescence and in adulthood. We anesthetized mice with isoflurane and acquired whole-brain images using a Bruker BioSpec 7-T spectrometer. We acquired brain images using the standard Bruker TrueFISP sequence,[18] with a repetition time of 5.2 ms, echo time of 2.6 ms, field-of-view of 18 mm × 18 mm × 9 mm, and matrix size of 128 × 128 × 64, producing images with 141 µm isotropic voxels. Total scan time for each mouse was less than 40 minutes.

Brain images were digitally aligned using linear image registration, followed by nonlinear registration with iterative template refinement encapsulated into a custom pipeline,[19–23] implemented in Pydpiper.[24] Briefly, this pipeline uses the advanced neuroimaging tools (ANTs) registration algorithm to align individual images toward an initial model, a 125 µm isotropic resolution MRI mouse brain template.[25,26] Once roughly aligned, the template is discarded and the individual images are further aligned to each other to create an iteratively refined, consensus average brain model from the 54 individual images. The Jacobian determinants of the final transformation fields needed to align the model to each individual brain image represent the local volume ratio at each voxel of each individual image, compared with the consensus average. Practically, they represent the extent to which brain elements (voxels) in an individual brain are larger or smaller than the group average.

We registered a previously constructed atlas of the mouse brain, generated by combining MRI-based segmentation atlases for different brain regions,[27–30] to the average brain model to determine the volumes of the 182 anatomic regions included in the atlas and for comparison of volumes between *DCC*-haploinsufficient and wild-type mice. We obtained the volume of each anatomic region for each brain at each age by summing the Jacobian determinants for the voxels within each region.

Methodological validation

We first examined the regions of interest from our previous report,[31] which used manual segmentation to measure only select brain regions, namely the anterior cingulate, prelimbic, and infralimbic subregions of the prefrontal cortex, the dorsal striatum, the nucleus accumbens, and the hippocampus. We employed the same statistical approach, mixed-effects analysis of variance (ANOVA),[31] to compare the volumes of our preselected regions of interest between *DCC*-haploinsufficient and wild-type mice. We included age as a fixed effect and mouse identification number as a random effect to account for repeated measurements.

We included the ventral tegmental area as a region of interest because it is the source of mesocorticolimbic dopamine projections that express DCC and innervate the frontal regions listed above. We also included the orbital subregions of the prefrontal cortex, the orbitofrontal and insular cortices, as they have protracted dopamine development during adolescence.[10]

Unbiased whole-brain volumetric analysis

We conducted mixed effects ANOVAs for age and genotype for each neural structure included in the MRI-based segmentation atlas[30] and for each voxel. For post hoc analyses, we conducted voxel-wise analyses separately for the adolescent and adult images, and compared the number of affected voxels between adolescents and adults using a pairwise *t* test. Throughout these analyses, when analyzing across both adolescent and adult measurements, we included age as a fixed effect and mouse identification number as a random effect to account for repeated measurements. For all analyses involving more than 2 comparisons of means, we adjusted *p* values using the false discovery rate (FDR) with a threshold of 5%.[32] Volumes in the results are presented in μL for clarity and were converted from voxels using the volume of a voxel (141 μm^3 or around 2.8×10^{-3} μL).

Overlap with structural connectivity

To test whether the spatial patterns of volume changes in *DCC* haploinsufficiency reflected the spatial organization of the mesocorticolimbic dopamine system, we used the Allen Institute for Brain Science's Mouse Brain Connectivity Atlas data sets on viral tracing.[33] If *DCC* haploinsufficiency induced widespread neuroanatomical changes in adolescence, we would not expect the spatial pattern of those changes to correlate with the dopamine system. However, if the changes were primarily localized to the dopamine system, we would expect such a correlation.

Briefly, the Allen Institute viral tracing data set consists of a series of injections of recombinant adeno-associated viruses that express enhanced green fluorescent protein. The tracer virus is injected into a variety of brain regions of adult mice, including Cre (cyclization recombination) lines targeting specific cell types. The tracer does not cross synapses, and thus describes direct neuronal connectivity.[34] We obtained the data in a processed form, gridded at an isotropic resolution of 50 μm and aligned to a template (Common Coordinate Framework version 3 [CCFv3])[35], from the Allen Institute's application programming interface.

Previously, for small injection volumes, we observed a relationship between tracer injectate volume and length of projection tract detected.[36] Therefore, here, we considered only the 1309 viral tracing experiments with more than 0.1 mm^3 of injectate. We computed the binary overlap between voxels that showed a significant difference in Jacobian determinant (i.e., local volume) between wild-type and *DCC*-haploinsufficient genotypes, thresholded at a *t* statistic corresponding to a FDR of 5%, and voxels that contain a tracer signal, thresholded at a projection density of 0.05. We obtained the map of *t* statistics describing volumetric changes caused by *DCC* haploinsufficiency from the linear mixed-effects model combining both adolescent and adult data sets, aligned to the Allen Institute's CCFv3 template using ANTs. We analyzed volume increases caused by *DCC* haploinsufficiency separately from volume decreases. Considering the tracer data as ground truth, we quantified overlap as both the sensitivity (i.e., proportion of voxels with a tracer signal that also showed a volume difference) and positive predictive value (i.e., proportion of voxels with volume differences that also showed a tracer signal).

We examined this overlap for an individual tracer experiment, Allen Brain Connectivity experiment 156314762, which targeted the ventral tegmental area in a mouse line transfected by tyrosine hydroxylase (TH)–internal ribosome entry site (IRES)–Cre estrogen receptor (CreER). This is the only experiment available that specifically targeted ventral tegmental area dopamine neurons; it was conducted in a male mouse. We quantified statistical significance by comparing the sensitivity and positive predictive values obtained against the distribution of sensitivities and positive predictive values for all 1309 Allen Brain Connectivity experiments considered in our analyses.

We also analyzed a set of 37 experiments that targeted the mesocorticolimbic dopamine system more broadly, including pre- and postsynaptic components. These experiments were conducted in dopamine receptor (DRD1, DRD2, or DRD3-specific) Cre mouse lines, and TH Cre mouse lines, and include experiments involving both male and female mice. We ranked the sensitivities and positive predictive values of the 37 tracing experiments against the values of all 1309 experiments, and used the Mann–Whitney *U* test to determine the *p* value.

Structural covariance

To assess structural covariance among our regions of interest, we first averaged the map of *DCC* haploinsufficiency–associated *t* statistics obtained from the linear mixed-effects model with a version mirrored across the midline, resulting in a bilaterally symmetric map of *t* statistics. We then generated masks for regions of significant volume change by thresholding at a *t* statistic corresponding to an FDR of 5%. We computed volumes for resulting clusters of voxels that overlapped with the regions of interest chosen a priori and further normalized volumes (separately for adolescents and adults) by regressing out the main effects of genotype and whole-brain volume. We assessed structural covariance by regressing the normalized volumes against each other separately for adolescent and adult data.[37]

Overlap with gene expression

To identify potential molecular mechanisms that might underlie the volumetric changes observed in *DCC*-haploinsufficient mice, we linked the Allen Institute's data on spatial gene expression to the spatial volumetric differences we observed in our MRI brain images. This analysis sought to identify specific genes whose spatial expression patterns in the brain predicted the volumetric changes associated with *DCC* haploinsufficiency, and gene modules that were enriched for these genes.[38] We used the Allen Developing Mouse Brain Atlas, which characterizes the expression patterns of 2104 genes related to neurodevelopment at 3 early postnatal ages (postnatal day 4, 14, and 28).[39] We obtained expression

data for all 3 available ages to contrast the relationship of pre-adolescent and adolescent gene expression on the neuroanatomical phenotype. We normalized gene expression data independently at each voxel and for each age by regressing out the total amount of gene expression, and mapped these data onto the common CCFv3 template to allow for comparisons with our structural data. Additional details regarding the sourcing of spatial gene expression data can be found in Lindenmaier and colleagues' article.[40]

Correlation between structural changes and gene expression for genes of interest

For each gene we computed the Spearman correlation between normalized spatial gene expression and the structural volume difference between *DCC*-haploinsufficient and wild-type mice, as quantified by the *t*-statistic map. Separately for each age, we ranked all available genes by correlation to determine which genes were most and least correlated with the *DCC*-haploinsufficient phenotype. Focusing on 3 genes of interest selected a priori (*DCC*, *NTN1*, and *UNC5*, which encodes the uncoordinated-5 receptor), we examined the rank order of these genes relative to all other available genes, hypothesizing that these genes would appear at the extreme ends of the ranked list.

Spatial gene enrichment

Gene modules are biologically relevant terms that are annotated with sets of genes, a prominent example being the set of gene ontology (GO) terms maintained by the GO Consortium.[38,41,42] We obtained a set of modules that combined GO terms with pathways from the Bader laboratory.[42] Using the list of genes ranked by their Spearman correlation with the *DCC*-haploinsufficient phenotype, we examined which modules contained genes that were preferentially distributed at the extreme ends of this ranked list.

Following the methods described by Ritchie and colleagues,[43] we first filtered the gene set to remove extremely large (i.e., generic) and extremely small modules, retaining those that contained between 10 and 200 genes (inclusive). To quantify enrichment given a ranked list of genes, we built on the area under the receiver operating characteristic curve (AUC), which is closely related to the *U* statistic from the Mann–Whitney *U* test. Briefly, for a given module, this statistic is calculated by computing the area under a curve formed by plotting the cumulative distribution of genes within the module as a function of rank; therefore, the AUC is a measure of how unevenly the genes within the module are distributed.

Motivated by the idea that both positive and negative correlations are meaningful, we used a modified version of the AUC. We split the ranked list in half, computed the AUC separately for both of these ordered lists of genes (with top rank being defined as the most extreme ends of the lists), and defined the bidirectional AUC as the mean of these 2 AUCs. Thus, for a given module, when the bidirectional AUC equalled around 1, genes within the module tended to be distributed at the ends of the ranked list, indicating a spatial enrichment pattern that is correlated with the *DCC* haploinsufficiency *t*-statistic map. If the bidirectional AUC equalled around 0, genes within the module tended to be clustered around the middle of the ranked list. If the bidirectional AUC equalled around 0.5, then genes within the module were evenly distributed across the list, indicating no relationship with the *DCC* haploinsufficiency *t*-statistic map.

To test which bidirectional AUC values were statistically significant, we used a randomization framework in which — for each module — a null distribution of bidirectional AUC values was constructed from an ensemble of 5000 random anatomic phenotypes. In our case, we generated random phenotypes by drawing 10 random genes at a time and computing the average spatial expression; this approach accounted for within-module coexpression and spatial autocorrelation that must be accounted for to avoid biased *p* values.[44] We first analyzed gene modules that contained our term of interest (netrin-1), using uncorrected *p* values. We then analyzed the complete suite of all gene modules using FDR-corrected *p* values.

Data and code

We conducted all analyses in the R statistical computing environment using the MRI analysis package (RMINC).[44,46] All data and code use in these analyses are available through the Open Science Framework (doi: 10.17605/OSF.IO/H64QF).

Ethics approval

All experiments were performed in accordance with the Canadian Council of Animal Care and the McGill University and Douglas Mental Health University Institute Animal Care Committee.

Results

Regional differences in neuroanatomical volumes between male DCC*-haploinsufficient and wild-type mice*

We included 11 *DCC*-haploinsufficient mice and 16 wild-type littermates, all males. We obtained MRI scans first during adolescence (postnatal day 33 ± 2), and then again in adulthood (postnatal day 75 ± 15). As an initial validation of our methods, we automated the measurement of the same structures previously measured using manual segmentation.[31] Using an MRI-based segmentation atlas and our automated segmentation algorithm, we found significant effects of age and genotype in the nucleus accumbens ($t = 6.21$, $q < 0.0001$ for age; $t = –2.99$, $q = 0.02$ for genotype; Figure 1) and in the hippocampus ($t = 6.80$, $q < 0.0001$ for age; $t = –2.67$, $q = 0.04$ for genotype; Figure 1). We did not find significant effects of genotype in the dorsal striatum ($t = 2.03$, $q = 0.1$) or in the anterior cingulate ($t = 0.63$, $q = 0.5$), prelimbic ($t = –0.23$, $q = 0.8$), and infralimbic ($t = –0.76$, $q = 0.4$) subregions of the medial prefrontal cortex (Figure 1). However, these regions did show significant effects of age (respectively, $t = 6.79$, $q < 0.0001$; $t = –5.84$, $q < 0.0001$; $t = –6.70$, $q < 0.0001$; $t = –3.26$,

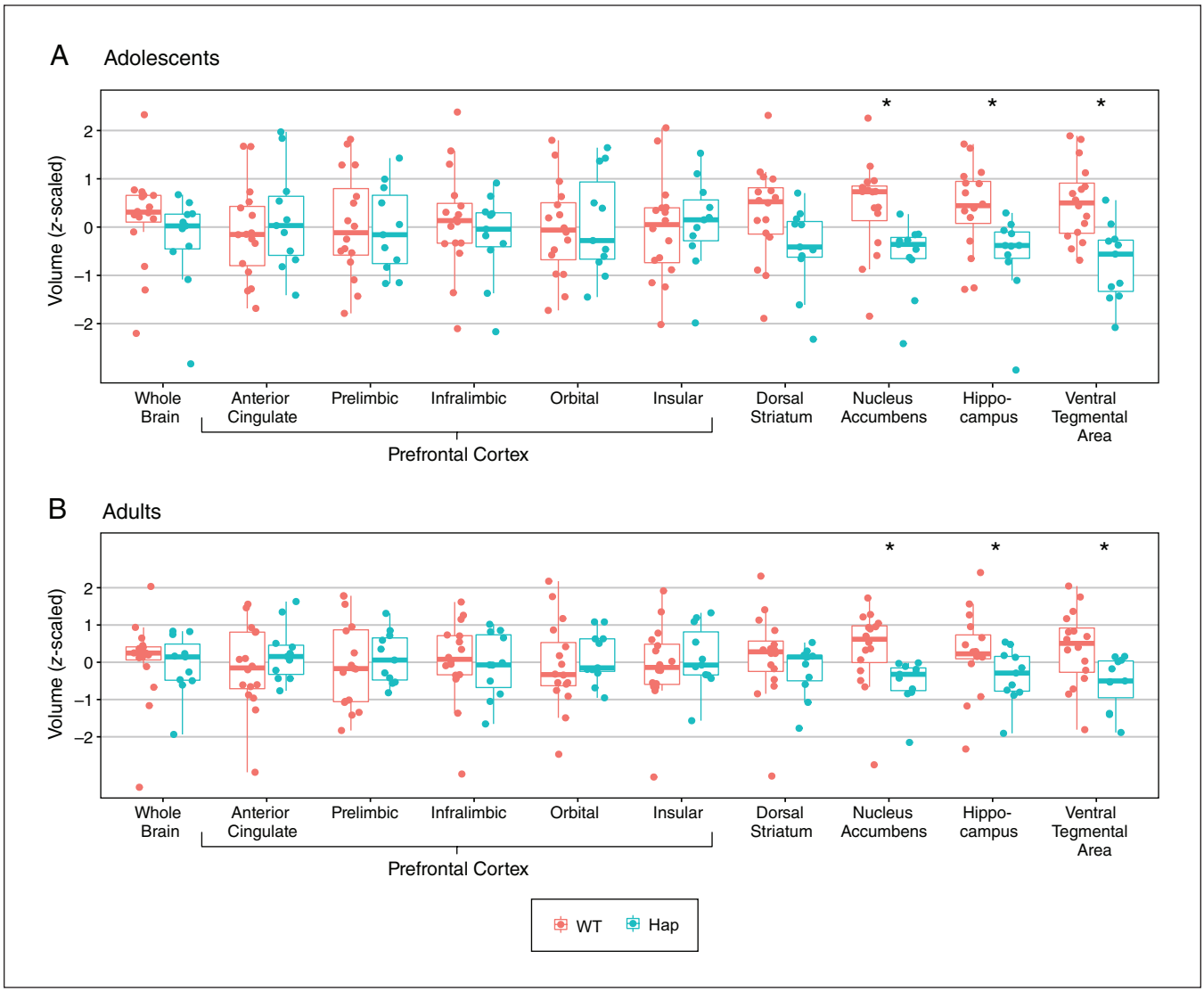

Figure 1: The effect of *DCC* haploinsufficiency on the volumes of brain regions of interest in (A) adolescence and (B) adulthood. Prefrontal cortex subregions and the dorsal striatum showed no volumetric differences between the 2 genotypes, while the other regions of interest were smaller in *DCC*-haploinsufficient (Hap) mice (n = 11) than in wild-type (WT) mice (n = 16). Box plots show median (thick horizontal lines), upper and lower quartiles (thin horizontal lines), minimums (lower whiskers), and maximums (upper whiskers). Data for the whole brain are also presented for comparative purposes. Adolescent and adult data are presented separately for clarity; however, the significant differences indicated by asterisks were determined using a mixed-effects analysis of variance that incorporated both age and genotype as independent variables. All data were centred and scaled such that all means equal 0 and all standard deviations equal 1.

q = 0.004). In all cases, affected brain regions were smaller in *DCC*-haploinsufficient mice than wild-type mice, and larger in adult mice than adolescent mice. These results are qualitatively identical to those we observed using manual segmentation.[31]

We looked at the ventral tegmental area because it is where cell bodies of mesocorticolimbic dopamine neurons are located. We found significant effects of age (t = 5.50, q < 0.0001) and genotype (t = –3.53, q = 0.01; Figure 1). We also looked at the orbital and insular subregions of the prefrontal cortex, which also receive mesocortical dopamine innervation in adolescence.[10] In the orbital prefrontal cortex, we found a significant effect of age (t = –6.24, q < 0.0001) but not genotype (t = 0.31, q = 0.8; Figure 1), and in the insular region we did not find significant effects of age (t = –0.97, q = 0.3) or genotype (t = 0.32, q = 0.8; Figure 1). In all cases, affected brain regions were smaller in *DCC*-haploinsufficient mice than wild-type mice and larger in adult mice than adolescent mice. We did not find significant interaction terms in any cases.

Next, we checked whether *DCC* haploinsufficiency affected whole-brain volume. We found no effect of genotype on brain volume (t = 0.59, p = 0.4; Figure 1), an effect of age — with the brain being larger in adulthood (t = 40.57, p < 0.0001) — and no interaction between variables (t = 2.65, p = 0.1).

After looking specifically at our regions of interest, we sought to evaluate differences across the whole brain between *DCC*-haploinsufficient and wild-type mice. Following adjustment of *p* values for multiple comparisons using an FDR of 5%, no structure showed a significant effect of genotype. A table of these results is available as Appendix 1, Supplementary Table 1, available at www.jpn.ca/lookup/doi/10.1503/jpn.230106/tab-related-content..

Subregional differences in volumes between male DCC*-haploinsufficient and wild-type mice*

We conducted linear mixed-effects models comparing the volumes of *DCC*-haploinsufficient and wild-type mice at each voxel across the entire brain. This dramatically increased the number of comparisons; however, this method can detect volumetric differences that do not substantially affect entire regions. Given the large number of comparisons, we adjusted our significance threshold using FDR. We found numerous voxels that were either larger or smaller among *DCC*-haploinsufficient mice compared with wild-type mice (Figure 2). Many of these voxel-wise differences were found in brain structures that, overall, were not different between genotypes (e.g., the prefrontal cortex).

When analyzing adolescents and adults separately, fewer voxels per brain region were larger ($t = 3.83$, $p = 0.0002$) or smaller ($t = 4.35$, $p < 0.0001$) among *DCC*-haploinsufficient mice in adulthood compared with adolescence, consistent with dynamic neural changes occurring in the adolescent brain. A complete table of anatomic locations that we found to be larger and smaller in *DCC*-haploinsufficient mice is available as Appendix 1, Supplementary Table 2.

As the same mice were imaged in adolescence and adulthood, we are also able to analyze and visualize brain development at the level of the individual. To this end, we identified the voxels most affected by *DCC* haploinsufficiency, as estimated by those voxels for which the comparison of overall volume difference between *DCC*-haploinsufficient and wild-type mice had an associated *p* value of less than 0.001. The results of this analysis are presented in Appendix 1, Supplementary Figure 1.

We observed clusters of significant voxels within our regions of interest (Table 1). In fact, visual examination of the *t* statistic neuroanatomical map (Figure 2) showed that the effects of *DCC* haploinsufficiency appear to be largely restricted to our regions of interest, comprising the cell body and terminal regions of mesocorticolimbic dopamine neurons. The subregions of the prefrontal cortex, which did not show significant volumetric changes at the region level, still included significantly altered voxels. Voxels that were larger in *DCC*-haploinsufficient mice were detected in the anterior cingulate and orbital subregions of the prefrontal cortex, along with smaller numbers of voxels in the insular and prelimbic subregions. We also found a small number of voxels that were smaller in *DCC*-haploinsufficient mice in the infralimbic subregion of the prefrontal cortex. Furthermore, we observed smaller voxels in the nucleus accumbens, hippocampus, and ventral tegmental area. Interestingly, the dorsal striatum showed large numbers of both larger and smaller voxels. Visual examination of the voxel maps suggested that the larger voxels were located more ventrally and posteriorly, while the smaller voxels were more dorsal and anterior (Figure 2).

Voxels affected by *DCC* haploinsufficiency were disproportionately represented in the mesocorticolimbic dopamine system. Considering both the adolescent and adult data together, we found similar proportions of larger voxels within our regions of interest as across the rest of the brain. However, the proportion of smaller voxels within our regions of interest was 3 times that found in the rest of the brain (Table 2). Similar patterns remained when we examined the adolescent and adult ages separately. From adolescence to adulthood, there was a substantial reduction in the proportions of voxels that were affected by *DCC* haploinsufficiency both within and outside of our regions of interest (Table 2).

Regions with volume changes associated with DCC *haploinsufficiency and dopamine projections*

To formalize our comparison of regions affected by *DCC* haploinsufficiency and regions that receive dopamine projections, we computed the binary overlap between the *DCC*-haploinsufficient phenotype (our MRI data, quantified as an anatomic map of *t* statistics; Figure 3A, lefthand column) and voxels that showed a fluorescent tracer signal in an experiment that labelled dopamine axons originating from the ventral tegmental area (Allen Institute connectivity experiment 156314762; Figure 3A, middle column). Connectivity data were considered as ground truth, and the sensitivity and positive predictive value showed significant overlap between regions that were smaller in *DCC* haploinsufficiency and those that receive dopamine projections from the ventral tegmental area (Figure 3B). However, there was no relationship between larger regions and dopamine projections. We found similar results when comparing the *DCC*-haploinsufficient phenotype with the set of 37 dopamine-targeting tracer experiments (Figure 3C, righthand column). In this case, the *t*-statistic map of volume decreases was significantly sensitive to the presence of a tracer signal, but did not predict connectivity (Figure 3C).

DCC *haploinsufficiency and coordination in male adolescent brain development*

Structural covariance — the correlated variation in volumes between pairs of structures — is thought to be a signature of coordinated neurodevelopment and connectivity.[37,47,48] We assessed structural covariance between our regions of interest in wild-type mice, separately in adolescence and adulthood, and measured how that covariance was altered by *DCC* haploinsufficiency.

In adolescence, we found positive covariance (enlargement of 1 region correlated with enlargement of another

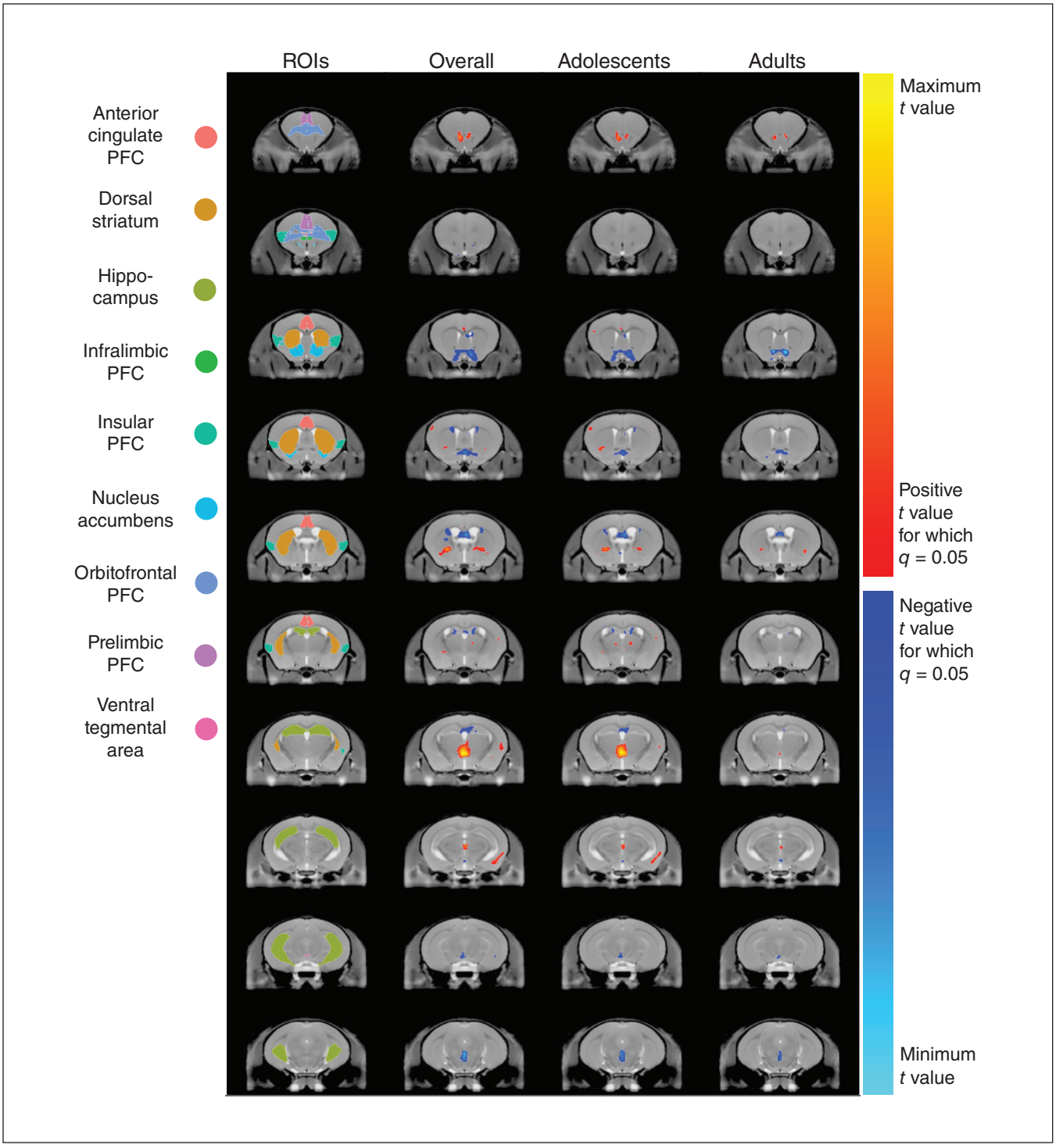

Figure 2: The effect of *DCC* haploinsufficiency on local brain anatomy in mice. Coronal sections are presented in anterior–posterior order from top to bottom in each column. Regions of interest (ROIs) are coloured in sequential coronal sections on the consensus model average of a mouse brain generated in this study. For columns 2, 3, and 4, warm-coloured voxels indicate anatomic locations that are larger ($q < 0.05$) in *DCC*-haploinsufficient mice than wild-type mice and cool-coloured voxels indicate locations that are smaller in *DCC*-haploinsufficient mice. Although this analysis was conducted across the entire brain, it is notable that there is substantial overlap between altered voxels and our predetermined ROIs. Column 2 demonstrates anatomic differences in *DCC*-haploinsufficient mice overall, as determined by a 2-way mixed-effects model with age and genotype as factors. Column 3 compares genotypes in adolescence, while column 4 compares genotypes in adulthood. All neuroanatomical differences between genotypes are more prominent in adolescence, with some being completely ameliorated by adulthood. PFC = prefrontal cortex.

Table 1: Volumetric effects of *DCC* haploinsufficiency in regions of interest*

	Overall		Adolescents		Adults		
Region of interest	Larger volume, µL	Smaller volume, µL	Larger volume, µL	Smaller volume, µL	Larger volume, µL	Smaller volume, µL	Total volume, µL
Anterior cingulate PFC	0.233	0.003	0.168	0.000	0.003	0.000	7.843
Prelimbic PFC	0.006	0.000	0.014	0.000	0.000	0.000	3.737
Infralimbic PFC	0.000	0.039	0.000	0.011	0.000	0.000	0.782
Orbital PFC	0.146	0.000	0.073	0.000	0.006	0.000	10.476
Insular PFC	0.053	0.000	0.000	0.000	0.000	0.000	11.353
Dorsal striatum	1.233	1.474	0.656	0.342	0.146	0.000	30.684
Nucleus accumbens	0.000	1.589	0.000	0.880	0.000	0.833	5.685
Hippocampus	0.000	1.418	0.000	0.830	0.000	0.090	28.753
Ventral tegmental area	0.000	0.109	0.000	0.104	0.000	0.028	0.174

PFC = prefrontal cortex.
*Volumes that were either larger or smaller in mice with *DCC* haploinsufficiency are indicated overall (in an analysis combining both adolescent and adult data sets) and separately by age class. Total volume indicates the volume of the whole structure, including parts unaffected in *DCC* haploinsufficiency, in an average including both adolescents and adults. Within a brain region, some subregions can be larger while others are smaller. Therefore, for each brain region, we identified voxels that increased and voxels that decreased in volume relative to wild-type mice. Voxels that were increased in volume were summed separately from voxels that were decreased in volume. This resulted in volume estimates of both larger and smaller portions of the same brain region.

Table 2: Volumetric effects of *DCC* haploinsufficiency in the mesocorticolimbic dopamine system and the rest of the brain*

	Overall		Adolescents		Adults	
Region	Larger volume, %	Smaller volume, %	Larger volume, %	Smaller volume, %	Larger volume, %	Smaller volume, %
Regions of interest	1.74	4.84	0.94	2.26	0.16	0.99
Rest of the brain	2.11	1.65	1.49	1.08	0.18	0.44
Whole brain	2.06	2.14	1.40	1.26	0.17	0.52

*Percentages of the total volumes that were affected (either larger or smaller) in mice with *DCC* haploinsufficiency are indicated overall (considering both adolescent and adult data sets) and separately for adolescents and adults. Our regions of interest, which describe the mesocorticolimbic dopamine system, were disproportionately affected compared with the rest of the brain. Adolescents were disproportionately affected compared with adults.

region) between the ventral tegmental area and medial accumbens, as well as between the dorsal striatum and the hippocampus. We found negative covariance (enlargement of 1 region correlated with diminution of another region) between the ventral tegmental area and the lateral accumbens, the hippocampus, and the medial accumbens, as well as between the dorsal striatum and prefrontal cortex (Figure 4A). In adolescent *DCC*-haploinsufficient mice, we found that the negative covariance between the ventral tegmental area and lateral accumbens was diminished (Figure 4A). That is, *DCC* haploinsufficiency resulted in a dissociation of volumetric changes between the ventral tegmental area and accumbens in adolescence.

In adulthood, both the positive covariances we observed in adolescence (between the ventral tegmental area and medial accumbens, and between the dorsal striatum and the hippocampus) were maintained in wild-type mice (Figure 4B). The negative covariance between the hippocampus and medial accumbens was also maintained, and there were additional negative covariances between the dorsal striatum and both the ventral tegmental area and lateral accumbens. In contrast with adolescence, none of the covariances observed in the adult mouse brain were affected by *DCC* haploinsufficiency (Figure 4B).

DCC *haploinsufficiency phenotype and expression of* DCC, NTN1, *and* UNC5 *in male mice*

We compared the *DCC*-haploinsufficient phenotype map (our MRI data, quantified as an anatomic map of *t* statistics) with data from the Allen Institute that mapped gene expression onto the mouse brain at 3 early postnatal ages (postnatal days 4, 14, and 28). We examined the spatial expression patterns of our genes of interest (*DCC*, *NTN1*, and *UNC5*) relative to the expression of the other genes included in the atlas. Using the Spearman coefficient, we computed the spatial correlations between *DCC*-associated volume change (represented by the *t* statistic) and normalized gene expression for each gene of interest. We ordered all genes in the Allen Developing Mouse Brain Atlas by increasing Spearman coefficient. Genes close to the top of the list (rank approaching 1) were positively correlated with the *DCC*-haploinsufficient phenotype map, while those at the bottom of the list (rank approaching –1) were inversely correlated with the phenotype map. Comparing *DCC*, *NTN1*, and the 4 homologues of *UNC5* to the rest of the genes included in the atlas, we found that these genes were frequently ranked at the extreme ends of the distribution (Figure 5). At postnatal day 4, *DCC* and *NTN1* expression were negatively correlated with the map, while *UNC5C* was positively correlated with the map. At

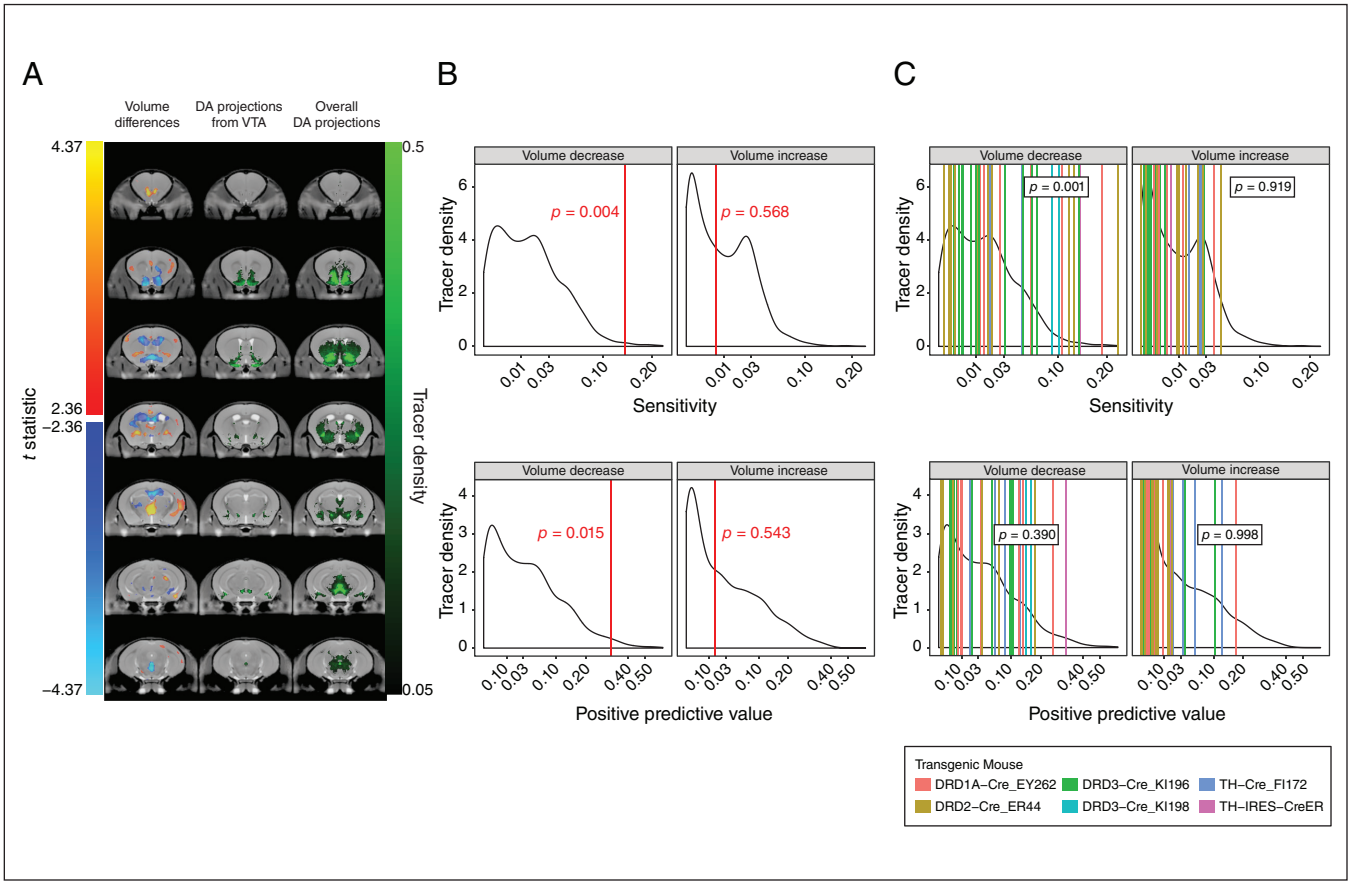

Figure 3: Volume differences in relation to connectivity. (A) Volume differences associated with *DCC* haploinsufficiency, computed from a linear mixed-effects model combining both ages, are shown in the left column. Red regions are larger and blue regions are smaller in *DCC* haploinsufficiency. The middle column shows a single viral tracing experiment, which labelled dopamine (DA) projections from the ventral tegmental area (VTA) (Allen Brain Connectivity experiment 156314762). The right column shows a maximum intensity projection of all 37 available Allen Brain Connectivity experiments that targeted the DA system. (B) Sensitivity (top) and positive predictive value (bottom) between *DCC* haploinsufficiency and DA projections from the VTA. The binary overlap between voxels showed significant negative and positive volume differences, when considering connectivity as ground truth. Sensitivity and positive predictive values were computed for the tracer experiment, illustrated as red vertical lines. Black curve shows distribution for all experiments. We calculated *p* values by comparing these values to those for all available viral tracing experiments (background density). Probability increases to the right; *p* values reflect the probability of obtaining values as extreme as the ones observed in relation to the background distribution. (C) Sensitivity (top) and positive predictive value (bottom) between *DCC* haploinsufficiency and DA projections overall. The binary overlap for the set of experiments illustrated in the right column of panel A, which target the DA system, are shown in the same format as panel B, with *p* values computed using the Mann–Whitney *U* test. The underlying curve (in black) represents the sensitivity or positive predictive values of all available viral tracer experiments. The vertical lines (coloured) represent the sensitivity or positive predictive values of the 37 experiments that target the DA system. Probability increases to the right; *p* values reflect the probability of obtaining a distribution of values for the 37 experiments as extreme as the ones observed in relation to the background distribution. Cre = cyclization recombination, DRD = dopamine receptor, IRES = internal ribosome entry site, TH = tyrosine hydroxylase.

postnatal day 14, *DCC* expression remained negatively correlated with the map and *UNC5C* expression remained positively correlated with the map. At postnatal day 28, the correlations were weaker; none of the genes appeared to significantly predict the phenotype map. At all 3 ages, the expressions of *UNC5A*, *UNC5B*, and *UNC5D* remained close to the centre of the distribution, indicating a lack of correlation with the phenotype map. A full list of all genes from the Allen Developing Mouse Brain Atlas and their correlations is available in Appendix 1, Supplementary Table 3.

The genes examined in the Allen Developing Mouse Brain Atlas can be grouped into gene sets or modules. We considered a set of modules that combined GO terms from the biological process tree[49] with pathway terms obtained from the Bader laboratory.[42] After filtering out extremely large and small modules, we ended with 3564, 3561, and 3575 modules for postnatal day 4, 14, and 28 respectively. The number of modules per age varied because of differing numbers of genes within the Allen Institute's gene expression data sets. The modules included 4 associated with netrin-1 function, namely

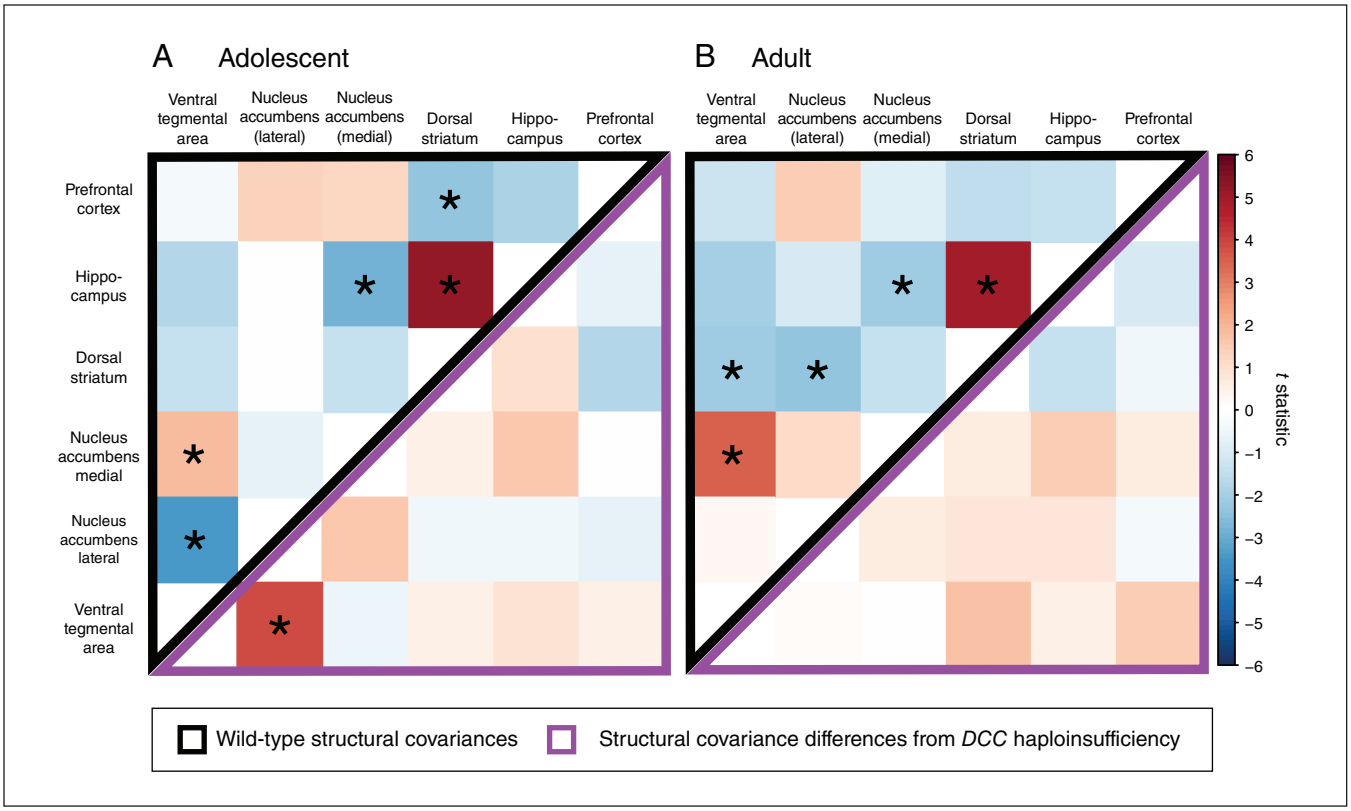

Figure 4: The effects of *DCC* haploinsufficiency on structural covariance between regions of interest. Values in the upper, black-bordered triangles assess the extent that a pair of regions covary in volume (*t* statistic for the main effect of structure) and values in the lower, purple-bordered triangles assess *DCC* haploinsufficiency–related differences in this structural covariance (*t* statistic for the structure–genotype interaction). Asterisks indicate structure pairs that covary significantly at a threshold of $q < 0.05$. (A) In adolescence, we observed covariance in volume between 5 structure pairs among wild-type mice (upper, black-bordered triangle). Among *DCC*-haploinsufficient mice, the negative structural covariance between the nucleus accumbens and the ventral tegmental area was reduced compared with wild-type mice (lower, purple-bordered triangle). (B) In adulthood, there was covariance between 5 structure pairs among wild-type mice (upper, black-bordered triangle). We did not see any effect of *DCC* haploinsufficiency on adult structural covariance (lower, purple-bordered triangle). Red regions are larger and blue regions are smaller in *DCC* haploinsufficiency.

the Pathway Interaction Database (PID) netrin pathway from the Molecular Signatures database curated gene sets, netrin-mediated signaling events from the National Cancer Institute–Nature Pathway Interaction Database, netrin-1 signaling from the Reactome Pathway Database (R-HSA-373752.2), and axon guidance mediated by netrin from the PANTHER Pathway database (P00009). All 4 modules contained our 3 genes of interest (*DCC*, *NTN1*, and *UNC5*). Two of these modules, the PID netrin pathway and netrin-mediated signaling events, completely overlapped in their gene annotations, effectively resulting in 3 modules related to netrin-1.

We computed spatial enrichment of these modules using a modified version of the AUC metric and calculated *p* values by testing against an ensemble of random phenotypes. We found that only the PID netrin pathway or netrin-mediated signaling events module was enriched with genes that correlate spatially with the *DCC*-haploinsufficient phenotype at postnatal day 4 (Figure 6). When exploring the rest of the modules, after adjusting *p* values for multiple comparisons, no module maintained a statistically significant level of enrichment (Appendix 1, Supplementary Table 4).

Discussion

Our unbiased approach to analyzing the neuroanatomical phenotype of the *DCC*-haploinsufficient mouse demonstrated that the mesocorticolimbic dopamine system was selectively affected, and that the phenotype was more pronounced in adolescence than in adulthood. By linking our data to the Allen Institute's public data sets, we were also able to detect potential molecular processes involved in generating this phenotype, with the *DCC*, *NTN1*, and *UNC5C* genes appearing to be involved, but not other genes linked to the netrin-1 signalling pathway. These happen to be the 3 netrin-1–related genes expressed by the mesocorticolimbic dopamine system,[4] further emphasizing the link between *DCC* haploinsufficiency and this system.

Using automated segmentation techniques, we found that the dorsal striatum of *DCC*-haploinsufficient mice had subregions that were significantly larger and others that were significantly smaller than wild-type controls. This may explain why Vosberg and colleagues[31] did not find an effect in this region in mice; the 2 effects we observe effectively cancel out when considering the volume of the dorsal striatum as a whole.

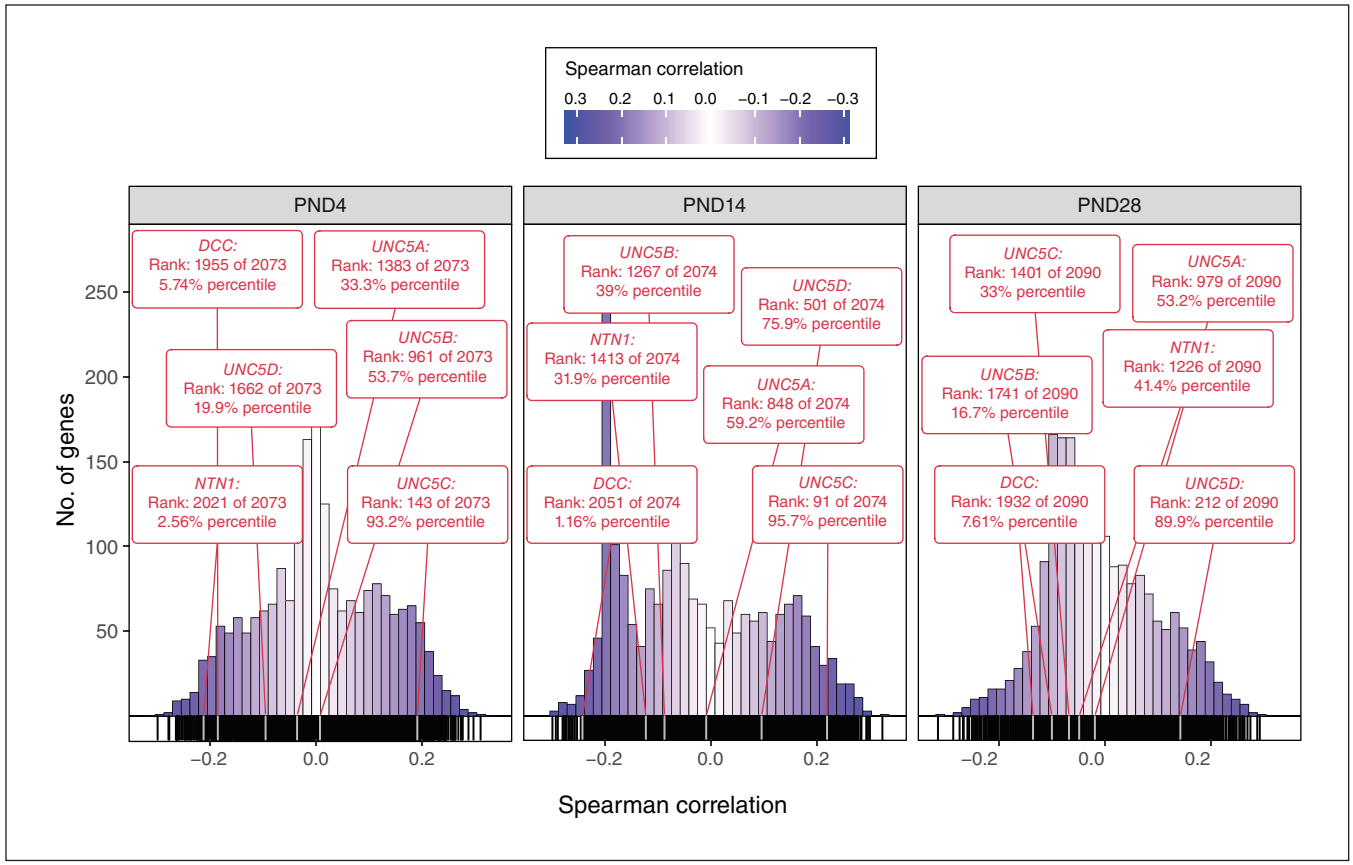

Figure 5: Frequency histograms of spatial correlations between the *DCC*-haploinsufficient phenotype and spatial gene expression at postnatal days (PNDs) 4, 14, and 28. For each age, a histogram of Spearman coefficients demonstrated the spatial similarity between normalized gene expression and the *DCC*-haploinsufficient phenotype (*t*-statistic map) for all genes in the Allen Institute's Developing Mouse Brain Atlas data set. Darker shades indicate a relatively strong relationship between gene expression and phenotype, while lighter shades indicate a relatively weak relationship. The positions and correlations of *DCC*, *NTN1*, and the 4 homologues of *UNC5* are indicated within these distributions. Positions near the left or right tails of the distribution indicate that the genes were negatively or positively correlated with the *DCC*-haploinsufficient phenotype, respectively.

Vosberg and colleagues[31] did not find a volumetric effect in the mouse prefrontal cortex; however, they did find significant increases in prefrontal cortex volume among human adults with *DCC* haploinsufficiency. In the present study, we found substantial areas of enlargement within most mouse prefrontal cortex subregions in *DCC* haploinsufficiency even though we did not find an effect on the overall volume in the prefrontal cortex. Nonetheless, parallel increases in prefrontal cortex volume with *DCC* haploinsufficiency among humans and mice show that the *DCC*-haploinsufficient mouse model is substantially more similar to the *DCC*-haploinsufficient phenotype in humans (as described in Vosberg and colleagues)[31] than previously understood.

The prefrontal cortex is important for controlling most complex cognitive processes and behaviours in humans, such as novelty seeking, drug seeking, and impulse control.[50] These behaviours are similarly altered among adult *DCC*-haploinsufficient humans and rodents.[6] Notably, at least in mice, these behavioural alterations only emerge in adolescence.[15]

Further understanding of *DCC* haploinsufficiency in humans will require novel multimodal approaches. In addition to the 3D gene expression data for the mouse brain that we used in this study, there are now 3D gene expression data sets available for the human brain through the Allen Brain Institute.[51] The Allen Institute's microarray brain atlases for *DCC* (probes A_23_P158708 and CUST_13856_PI416261804) reveal that the regions where we have detected the most substantial volumetric effects of *DCC* haploinsufficiency, namely the hippocampus, nucleus accumbens, and ventral tegmental area, have high levels of *DCC* mRNA expression in the adult human brain.

In the case of *DCC* haploinsufficiency, the development of human spatial gene expression data sets at multiple ages, including adolescence, is likely a key factor helping accelerate our understanding of this syndrome. The Allen Brain Institute's *Brainspan: Atlas of the Developing Human Brain* publishes *DCC* microarray data for limited brain regions in humans across ages.[52] The data (ENSG00000187323) reveal a general trend of decreasing *DCC* mRNA expression with

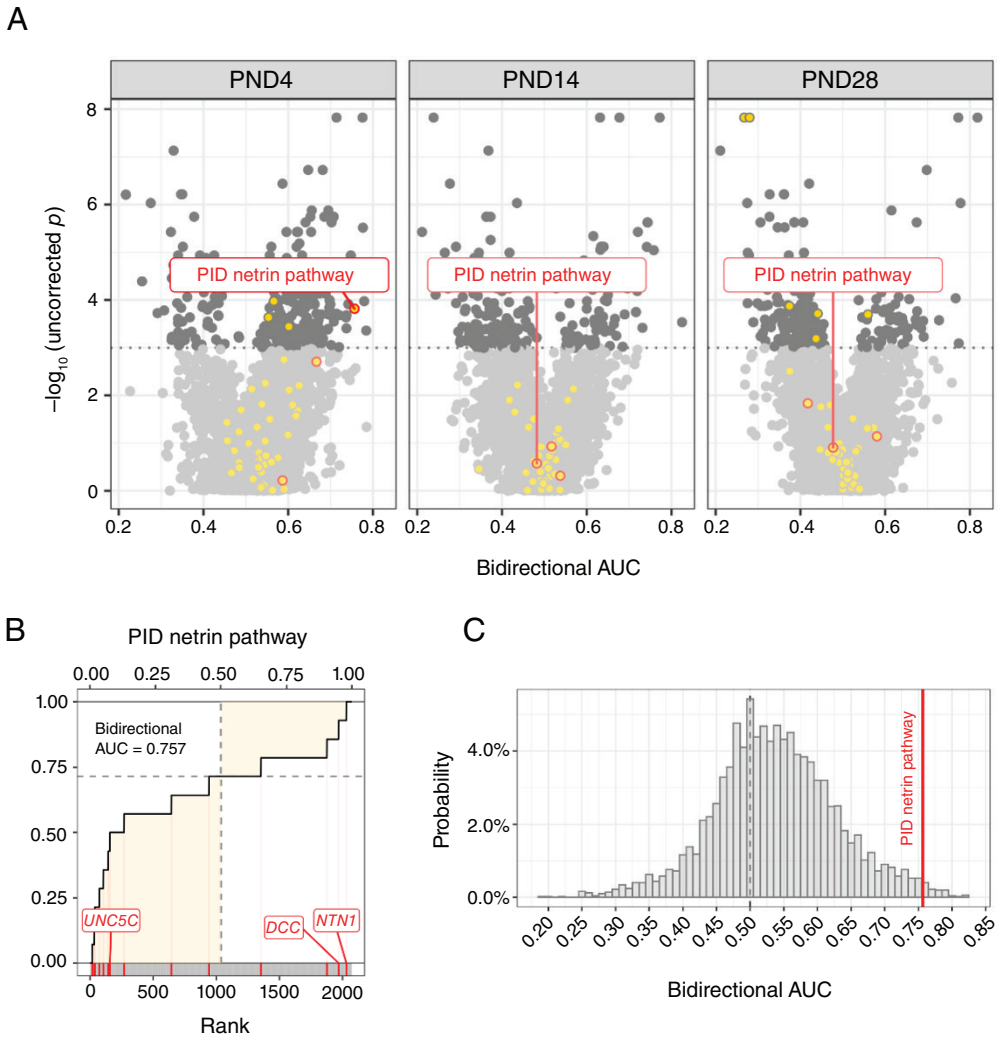

Figure 6: Spatial gene enrichment analysis using genes ranked by their correlation to the *DCC*-haploinsufficient neuroanatomical phenotype. (A) A volcano plot demonstrates the extent to which each gene module was enriched. Each point is a module, and those above the dotted line are statistically significant ($p < 0.05$) under a randomization approach. Points filled in yellow represent modules that contained at least 1 of our genes of interest (*DCC*, *NTN1*, and *UNC5*), and points circled in red are netrin-1–related modules that contain all 3 genes. Of the 3 modules that contain all 3 genes of interest, only the Pathway Interaction Database (PID) netrin pathway module at postnatal day (PND) 4 was enriched. (B) Bidirectional area under the receiver operating characteristic curve (AUC) for the PID netrin pathway module at PND4, constructed by going across the ranked list and incrementing when a gene within the module was found. The bidirectional AUC is represented as the proportion of the shaded area to the total area of the lower-left and upper-right quadrants and is a measure of how probably distributed genes within the module were in the provided ranked list. (C) The bidirectional AUC from the PID netrin pathway module at PND4, shown as a red line and compared with randomized AUC values obtained from a distribution of 5000 random phenotypes. The position of the module in this distribution was used to determine the *p* value.

increasing age, as we have previously shown in rodents.[53] However, notably, the striatum (which includes the nucleus accumbens) and the hippocampus maintain relatively high levels of *DCC* mRNA expression across the lifespan. As more data sets are generated, understanding genetic disorders, including *DCC* haploinsufficiency, will become easier and the development of potential treatment and mitigation strategies will be more streamlined. Indeed, research regarding the spatiotemporal expression of *DCC* gene co-expression networks using human data sets has highlighted their enrichment in mesocorticolimbic dopamine regions and dynamic patterns during adolescence.[54]

By comparing the volumetric effects of *DCC* haploinsufficiency within our regions of interest with the effects on the rest of the brain, we observed that the mesocorticolimbic dopamine system was disparately affected. We reinforced

this finding using anterograde tracers to locate the projection field of the ventral tegmental area's dopamine neurons, rather than a priori knowledge. The projection field of the dopamine system, identified through tracer studies, overlapped with areas that were smaller among *DCC*-haploinsufficient mice, although not regions that were larger. This is consistent with most regions known to receive these projections. However, the prefrontal cortex showed primarily larger areas among *DCC*-haploinsufficient mice, even though this area is known to receive dopamine input. We hypothesize that its sparse ventral tegmental area dopamine input is too diffuse to detect using the tracer data from the Allen Brain Connectivity Atlas.

The effects of *DCC* haploinsufficiency were substantially larger in the adolescent brain than the adult brain, which is consistent with the major remodelling of dopamine connectivity that occurs in adolescence and is largely governed by DCC receptors. In *DCC*-haploinsufficient mice, dopamine axons are misrouted during adolescence.[9] Here, we observed that volumetric differences largely mapped to the pattern of axon pathfinding. Regions from which axons are rerouted were smaller, and regions to which axons are rerouted were larger in *DCC*-haploinsufficient mice.

In this context, it is important to note that there was reduced structural covariance between the ventral tegmental area and the nucleus accumbens among adolescent *DCC*-haploinsufficient mice; these 2 structures represent the source and terminus of the most substantial dopamine projections of the mesolimbic system. The DCC receptors expressed on dopamine axons promote target recognition in the nucleus accumbens during adolescence.[11] If *DCC* expression by dopamine neurons is reduced, their axons fail to recognize the accumbens as their innervation target and continue to grow ectopically to the prefrontal cortex.[9,10] The reduction in covariance between the ventral tegmental area and the accumbens may reflect the failure of dopamine axons to correctly innervate the nucleus accumbens as a result of reduced *DCC* expression.

The volumetric changes we observed in *DCC*-haploinsufficient mice during adolescence were somewhat ameliorated by adulthood. Furthermore, the reduction in covariance between the nucleus accumbens and ventral tegmental area was no longer observed, suggesting that, by adulthood, there is no longer a discordance between the volumes of these 2 regions, perhaps because of compensatory processes. In adulthood, *DCC* haploinsufficiency does result in an altered behavioural phenotype, and we noted that some anatomic abnormalities remained as well, indicating that the *DCC*-haploinsufficiency phenotype was not transitory, but remained throughout life. However, the dynamic developmental processes that are altered, resulting in the phenotype, appear to be restricted to a small critical period in early adolescence.[55] The decrease in the volumetric effects of *DCC* haploinsufficiency observed between adolescence and adulthood could be the result of a compensatory mechanism or could result from the cessation of dynamic developmental processes during adolescence. This is a worthwhile avenue of further investigation.

We examined correlations in gene expression with the *DCC*-haploinsufficient phenotype to gain insight into potential genetic mechanisms mediating the anatomic changes we observed. Expression of *DCC*, as well as the expression of its ligand *NTN1* and the receptor with which it forms a complex, *UNC5C*, all showed patterns that correlated with the volumetric changes caused by *DCC* haploinsufficiency. Across the brain, in regions where *DCC* expression was high, we found volume loss in *DCC* haploinsufficiency. We found a similar, but weaker, pattern for *NTN1* expression. Although we examined all 4 homologues of *UNC5*, the only homologue to show an expression pattern that mirrored the *DCC*-haploinsufficient phenotype map was *UNC5C*, the homologue expressed by dopamine neurons in the ventral tegmental area.[56] Before adolescence, in regions where *UNC5C* expression was high, volume gain was observed in *DCC* haploinsufficiency. At postnatal day 28, no gene of interest, including *DCC*, correlated with the *DCC*-haploinsufficient phenotype. This is consistent with a recent study that found early adolescence (starting at postnatal day 21) as the critical period for alterations to mesocorticolimbic dopamine development among male mice.[55] Postnatal day 28 is likely past the critical period for axon guidance mechanisms to shape the male mesocorticolimbic dopamine system. Whether the same critical period exists among females is an important outstanding question.

We ran a spatial gene enrichment analysis to identify biological processes and pathways that might explain the patterns of volume change we observed. Of 3 pre-selected *NTN1*-related modules that contained all 3 genes of interest (*DCC*, *NTN1*, and *UNC5*), only 1 was significantly enriched with genes whose expression patterns correlated with the *DCC*-haploinsufficient neuroanatomical phenotype; after an exploratory approach that tested enrichment in more than 3000 other modules, no modules were significantly enriched after correction for multiple comparisons. We used an ensemble of random phenotypes to build a null distribution of enrichment (bi-directional AUC) values from which p values were computed to reduce bias, which might occur at the expense of sensitivity.[44] Nonetheless, this result suggests that the effect of *DCC* haploinsufficiency on neuroanatomy is a direct result of reduced presence of DCC receptors in the brain, rather than altering the expression of other genes related to netrin-1 function. Indeed, behaviour–gene expression correlation studies involving humans have indicated that DCC receptors act as a master organizer of adolescent mesocorticolimbic development and that variation in *DCC* expression alone can have cascading downstream effects.[57]

Limitations

Adolescent development proceeds differently between males and females, and the development of the mesocorticolimbic system is no exception.[58–62] In adults, both the architecture and function of the mesocorticolimbic dopamine system are sexually dimorphic,[3] indicating that the maturation of this system in adolescence occurs in a sex-specific manner. Studies of these processes among females are currently ongoing and are essential to understanding the neural foundations of the sex-specific aspects of adolescence development.

In addition, although adolescence is a critical period for mesocorticolimbic dopamine development, a subset of dopamine axons grows to the prefrontal cortex during both embryonic and early postnatal development.[63] Comparisons of MRI scans from earlier ages would help characterize the global effects of *DCC* haploinsufficiency on dopamine development and further determine whether *DCC* haploinsufficiency affects other neural networks at other developmental stages.

Finally, although we detected correlative effects between *DCC* haplosufficiency and the expression of *NTN1* and *UNC5C*, very little functional data were available to understand what this might mean in terms of neural connectivity or behaviour. Available data, which collected from adult mice only, suggest that *DCC* haploinsufficiency does not result in changes in the expression levels of either *NTN1* or *UNC5C*, and the same seems to be the case in *NTN1* haploinsufficiency.[14,64] Future experiments need to address whether *DCC* haploinsufficiency alters the expression of *NTN1* and *UNC5C* specifically during adolescence and what effects this may have on development, connectivity, and behaviour among rodents and humans.

Conclusion

Haploinsufficiency of *DCC*, where individuals have only 1 functional copy of the *DCC* gene, results in altered brain development, structure, and function.[3,4] The effects of *DCC* haploinsufficiency on neuroanatomy are disproportionately represented in the brain regions that constitute the mesocorticolimbic dopamine system, a system that is still undergoing major neuroanatomical change in adolescence. The neuroanatomical effects of *DCC* haploinsufficiency, both within and outside the mesocorticolimbic dopamine system, are more substantial in adolescence than in adulthood. Furthermore, *DCC* haploinsufficiency reduces the volumetric covariance between the ventral tegmental area and its primary innervation target, the nucleus accumbens, indicating a disruption in the coordinated development of these 2 closely linked regions. Gene expression maps suggest that these structural changes are a direct result of changes in *DCC* expression, supporting the concept of DCC as a master organizer of adolescent mesocorticolimbic development. The *DCC*-haploinsufficient mouse model provides insight into the consequences of *DCC* haploinsufficiency in humans, reveals molecular and cellular processes underlying adolescent brain maturation, and provides mechanistic clues relevant to the development of interventions for adolescence-associated psychiatric disorders.

Affiliations: From the Mouse Imaging Centre, Hospital for Sick Children, Toronto, Ont. (Hoops, Yee, Hammill, Wong, Lerch, Sled); the Department of Medical Biophysics, University of Toronto, Ont. (Hoops, Yee, Lerch, Sled); the Department of Psychiatry, McGill University, Montréal, Que. (Hoops, Flores); the Douglas Mental Health University Institute, Montréal, Que. (Hoops, Manitt, Flores); the Department of Chemistry, Memorial University, St. John's, N.L. (Hoops, Cahill); the Department of Neurology and Neurosurgery, McGill University, Montréal, Que. (Bedell, Flores); the Wellcome Centre for Integrative Neuroimaging, Centre for Functional MRI of the Brain, Nuffield Department of Clinical Neuroscience, University of Oxford, U.K. (Lerch); the Ludmer Centre for Neuroinformatics & Mental Health, McGill University, Montréal, Que. (Flores).

Competing interests: None declared.

Contributors: Daniel Hoops, Colleen Manitt, and Cecilia Flores contributed to the conception and design of the work. Yohan Yee, Sammi Wong, Barry Bedell, Lindsay Cahill, Jason Lerch contributed to data acquisition, analysis, and interpretation. Daniel Hoops and Cecilia Flores drafted the manuscript. All of the authors revised it critically for important intellectual content, gave final approval of the version to be published, and agreed to be accountable for all aspects of the work.

Funding: Daniel Hoops is supported by a postdoctoral fellowship from the National Science and Engineering Research Council of Canada (PDF 5171462018). Cecilia Flores is supported by the National Institute on Drug Abuse (R01DA037911), the Natural Science and Engineering Research Council of Canada (2982226), and the Canadian Institutes of Health Research (MOP 74709, PJT 190045). John Sled is supported by the Canadian Institutes of Health Research (PJT 169050, 152961, 375704).

References

1. Walker DM, Bell MR, Flores C, et al. Adolescence and reward: making sense of neural and behavioral changes amid the chaos. *J Neurosci* 2017;37:10855-66.
2. Juraska JM, Willing J. Pubertal onset as a critical transition for neural development and cognition. *Brain Research* 2017;1654:87–94.
3. Reynolds LM, Flores C. Mesocorticolimbic dopamine pathways across adolescence: diversity in development. *Front Neural Circuits* 2021;15:735625.
4. Hoops D, Flores C. Making dopamine connections in adolescence. *Trends Neurosci* 2017;40:709-19.
5. Srour M, Rivière JB, Pham JMT, et al. Mutations in *DCC* cause congenital mirror movements. *Science* 2010;328:592.
6. Vosberg DE, Leyton M, Flores C. The Netrin-1/DCC guidance system: dopamine pathway maturation and psychiatric disorders emerging in adolescence. *Mol Psychiatry* 2020;25:297-307.
7. Torres-Berrío A, Hernandez G, Nestler EJ, et al. The Netrin-1/DCC guidance cue pathway as a molecular target in depression: translational evidence. *Biol Psychiatry* 2020;88:611-24.
8. Manitt C, Eng C, Pokinko M, et al. dcc orchestrates the development of the prefrontal cortex during adolescence and is altered in psychiatric patients. *Transl Psychiatry* 2013;3:e338.
9. Reynolds LM, Pokinko M, Torres-Berrío A, et al. DCC receptors drive prefrontal cortex maturation by determining dopamine axon targeting in adolescence. *Biol Psychiatry* 2018;83:181-92.
10. Hoops D, Reynolds LM, Restrepo-Lozano JM, Flores C. dopamine development in the mouse orbital prefrontal cortex is protracted and sensitive to amphetamine in adolescence. *eNeuro* 2018;5:ENEURO.0372-17.2017-9.
11. Cuesta S, Nouel D, Reynolds LM, et al. dopamine axon targeting in the nucleus accumbens in adolescence requires netrin-1. *Front Cell Dev Biol* 2020;8:487.
12. Manitt C, Mimee A, Eng C, et al. The netrin receptor DCC is required in the pubertal organization of mesocortical dopamine circuitry. *J Neurosci* 2011;31:8381-94.
13. Hoops D, Grant A, Labelle-Dumais C, et al. Netrin-1 receptor deficiency protects against psychostimulant-induced behaviours in mice. *MSURJ* 2008;3:9-16.
14. Grant A, Hoops D, Labelle-Dumais C, et al. Netrin-1 receptor-deficient mice show enhanced mesocortical dopamine transmission and blunted behavioural responses to amphetamine. *Eur J Neurosci* 2007;26:3215-28.
15. Grant A, Speed Z, Labelle-Dumais C, et al. Post-pubertal emergence of a dopamine phenotype in netrin-1 receptor-deficient mice. *Eur J Neurosci* 2009;30:1318-28.

16. Avramescu RG, Flores C. We're not in Kansas anymore: ectopic dopaminergic terminals as an explanation for the positive symptoms in psychiatric pathology. *J Psychiatry Neurosci* 2023;48:E74-7.
17. Fazeli A, Dickinson SL, Hermiston ML, et al. Phenotype of mice lacking functional *Deleted in colorectal cancer (Dec)* gene. *Nature* 1997;386:796-804.
18. Miraux S, Massot P, Ribot EJ, et al. 3D TrueFISP imaging of mouse brain at 4.7T and 9.4T. *J Magn Reson Imaging* 2008;28:497-503.
19. Lerch JP, Sled JG, Henkelman RM. magnetic resonance neuroimaging, methods and protocols. *Methods Mol Biol* 2011;711:349-61.
20. Anacker C, Scholz J, O'Donnell KJ, et al. Neuroanatomic differences associated with stress susceptibility and resilience. *Biol Psychiatry* 2016;79:840-9.
21. Lerch JP, Yiu AP, Martinez-Canabal A, et al. Maze training in mice induces MRI-detectable brain shape changes specific to the type of learning. *Neuroimage* 2011;54:2086-95.
22. Kovacevic N. A Three-dimensional MRI atlas of the mouse brain with estimates of the average and variability. *Cereb Cortex* 2003;15:639-45.
23. Nieman BJ, van Eede MC, Spring S, et al. MRI to assess neurological function. *Curr Protoc Mouse Biol* 2018;8:e44.
24. Friedel M, van Eede MC, Pipitone J, et al. Pydpiper: a flexible toolkit for constructing novel registration pipelines. *Front Neuroinform* 2014;8:67.
25. Avants BB, Tustison NJ, Song G, et al. A reproducible evaluation of ANTs similarity metric performance in brain image registration. *Neuroimage* 2011;54:2033-44.
26. Avants BB, Tustison NJ, Wu J, et al. An open source multivariate framework for n-tissue segmentation with evaluation on public data. *Neuroinformatics* 2011;9:381-400.
27. Dorr AE, Lerch JP, Spring S, et al. High resolution three-dimensional brain atlas using an average magnetic resonance image of 40 adult C57Bl/6J mice. *Neuroimage* 2008;42:60-9.
28. Steadman PE, Ellegood J, Szulc KU, et al. Genetic effects on cerebellar structure across mouse models of autism using a magnetic resonance imaging atlas. *Autism Res* 2014;7:124-37.
29. Ullmann JFP, Watson C, Janke AL, et al. A segmentation protocol and MRI atlas of the C57BL/6J mouse neocortex. *Neuroimage* 2013;78:196-203.
30. Richards K, Watson C, Buckley RF, et al. Segmentation of the mouse hippocampal formation in magnetic resonance images. *Neuroimage* 2011;58:732-40.
31. Vosberg DE, Zhang Y, Menegaux A, et al. mesocorticolimbic connectivity and volumetric alterations in DCC mutation carriers. *J Neurosci* 2018;38:4655-65.
32. Genovese CR, Lazar NA, Nichols T. Thresholding of statistical maps in functional neuroimaging using the false discovery rate. *Neuroimage* 2002;15:870-8.
33. Oh SW, Harris JA, Ng L, et al. A mesoscale connectome of the mouse brain. *Nature* 2014;508:207-14.
34. Chamberlin NL, Du B, de Lacalle S, et al. Recombinant adeno-associated virus vector: use for transgene expression and anterograde tract tracing in the CNS. *Brain Res* 1998;793:169-75.
35. Wang Q, Ding SL, Li Y, et al. The Allen Mouse Brain Common Coordinate Framework: a 3D reference atlas. *Cell* 2020;181:936-953.e20.
36. Yee Y, Fernandes DJ, French L, et al. Structural covariance of brain region volumes is associated with both structural connectivity and transcriptomic similarity. *Neuroimage* 2018;179:357-72.
37. Lerch JP, Worsley K, Shaw WP, et al. Mapping anatomical correlations across cerebral cortex (MACACC) using cortical thickness from MRI. *Neuroimage* 2006;31:993-1003.
38. Carbon S, Douglass E, Dunn N, et al. The gene ontology resource: 20 years and still going strong. *Nucleic Acids Res* 2019;47:D330-8.
39. Sunkin SM, Ng L, Lau C, et al. Allen Brain Atlas: an integrated spatio-temporal portal for exploring the central nervous system. *Nucleic Acids Res* 2013;41:D996-1008.
40. Lindenmaier Z, Yeea Y, Kinman A, et al. Characterization of mice bearing humanized androgen receptor genes (*h/mAr*) varying in polymorphism length. *Neuroimage* 2021;226:117594.
41. Ashburner M, Ball CA, Blake JA, et al. Gene ontology: tool for the unification of biology. *Nat Genet* 2000;25:25-9.
42. Merico D, Isserlin R, Stueker O, et al. Enrichment map: a network-based method for gene-set enrichment visualization and interpretation. *PLoS One* 2010;5:e13984.
43. Ritchie J, Pantazatos SP, French L. Transcriptomic characterization of MRI contrast with focus on the T1-w/T2-w ratio in the cerebral cortex. *Neuroimage* 2018;174:504-17.
44. Fulcher BD, Arnatkeviciute A, Fornito A. Overcoming false-positive gene-category enrichment in the analysis of spatially resolved transcriptomic brain atlas data. *Nat Commun* 2021;12:2669.
45. Team RCR. A language and environment for statistical computing. R Foundation for Statistical Computing; 2014.
46. Lerch J, Hammill C, Eede M, et al. RMINC: statistical tools for medical imaging NetCDF (MINC) Files. 2016. Available: https://CRAN.R-project.org/package=RMINC (accessed 2017 Aug. 21).
47. Alexander-Bloch A, Giedd JN, Bullmore E. Imaging structural covariance between human brain regions. *Nat Rev Neurosci* 2013;14:322-36.
48. Evans AC. Networks of anatomical covariance. *Neuroimage* 2013;80:489-504.
49. The Gene Ontology Consortium, Carbon S, Douglass E, et al. The gene ontology resource: enriching a GOld mine. *Nucleic Acids Res* 2021;49:D325-34.
50. Fuster JM, editor. *The prefrontal cortex*. 5th ed. Amsterdam: Elsevier; 2015.
51. Hawrylycz MJ, Lein ES, Guillozet-Bongaarts AL, et al. An anatomically comprehensive atlas of the adult human brain transcriptome. *Nature* 2012;489:391-9.
52. Kang HJ, Kawasawa YI, Cheng F, et al. Spatio-temporal transcriptome of the human brain. *Nature* 2011;478:483-9.
53. Cuesta S, Restrepo-Lozano JM, Silvestrin S, et al. Non-contingent exposure to amphetamine in adolescence recruits miR-218 to regulate *Dcc* expression in the VTA. *Neuropsychopharmacology* 2018;43:900-11.
54. Restrepo-Lozano JM, Flores C, Silveira PP. Novel functional genomics approaches bridging neuroscience and psychiatry. *Biol Psychiatry Glob Open Sci* 2022;3:351-61.
55. Reynolds LM, Yetnikoff L, Pokinko M, et al. Early adolescence is a critical period for the maturation of inhibitory behavior. *Cereb Cortex* 2019;29:3676-86.
56. Manitt C, Labelle-Dumais C, Eng C, et al. Peri-pubertal emergence of UNC-5 homologue expression by dopamine neurons in rodents. *PLoS One* 2010;5:e11463-14.
57. Restrepo-Lozano JM, Pokhvisneva I, Wang Z, et al. Corticolimbic *DCC* gene co-expression networks as predictors of impulsivity in children. *Mol Psychiatry* 2022;27:2742-50.
58. Juraska JM. Changes in sex differences in neuroanatomical structure and cognitive behavior across the life span. *Learn Mem* 2022;29:340-8.
59. Becker JB, Chartoff E. Sex differences in neural mechanisms mediating reward and addiction. *Neuropsychopharmacol* 2019;44:166-83.
60. Juraska JM, Drzewiecki CM. Cortical reorganization during adolescence: what the rat can tell us about the cellular basis. *Dev Cogn Neurosci* 2020;45:100857.
61. Gulley JM, Juraska JM. The effects of abused drugs on adolescent development of corticolimbic circuitry and behavior. *Neuroscience* 2013;249:3-20.
62. Brown RE. *Neurodevelopmental pediatrics, genetic and environmental influences*. New York: Springer; 2023:179–212.
63. Kolk SM, Gunput RAF, Tran TS, et al. Semaphorin 3F is a bifunctional guidance cue for dopaminergic axons and controls their fasciculation, channeling, rostral growth, and intracortical targeting. *J Neurosci* 2009;29:12542-57.
64. Pokinko M, Moquin L, Torres-Berrío A, et al. Resilience to amphetamine in mouse models of netrin-1 haploinsufficiency: role of mesocortical dopamine. *Psychopharmacology (Berl)* 2015;232:3719-29.